ACS Catalysis

Research Article

pubs.acs.org/acscatalysis

Methane Oxidation on $Pd@ZrO_2/Si-Al_2O_3$ Is Enhanced by Surface Reduction of ZrO_2

Chen Chen,*[,†] Yu-Hao Yeh,[†] Matteo Cargnello,[‡] Christopher B. Murray,[‡,§] Paolo Fornasiero,[∥] and Raymond J. Gorte[†]

[†]Department of Chemical and Biomolecular Engineering, University of Pennsylvania, 231 South 34th Street, Philadelphia, Pennsylvania 19104, United States

[‡]Department of Chemistry, University of Pennsylvania, 231 South 34th Street, Philadelphia, Pennsylvania 19104, United States

[§]Department of Materials Science and Engineering, University of Pennsylvania, 3131 Walnut Street, Philadelphia, Pennsylvania 19104, United States

[∥]Department of Chemical and Pharmaceutical Sciences, ICCOM-CNR, Consortium INSTM, University of Trieste, via L. Giorgieri 1, 34127 Trieste, Italy

ABSTRACT: The catalytic properties of $Pd@ZrO_2$ core–shell catalysts supported on Si-modified alumina were studied for application to methane oxidation and compared to the analogous $Pd@CeO_2$ catalysts. In the absence of water (dry conditions), both $Pd@ZrO_2$ and $Pd@CeO_2$ were highly active and showed nearly identical reaction rates and thermal stabilities. However, unlike catalysts based on $Pd@CeO_2$, the $Pd@ZrO_2$ catalysts were also very stable in the presence of high concentrations of water vapor. By means of Coulometric titration and pulse-reactor studies, we demonstrate that ZrO_2 in contact with Pd can be reduced. Additionally, Coulometric titration showed that the Pd-PdO equilibrium at 600 °C is shifted to much lower $P(O_2)$ in the $Pd@ZrO_2$ catalyst compared to conventional Pd/ZrO_2 or Pd/Al_2O_3 catalysts. Because PdO is more active for methane oxidation, this observation provides a possible explanation for the superior performance of the $Pd@ZrO_2$ catalyst.

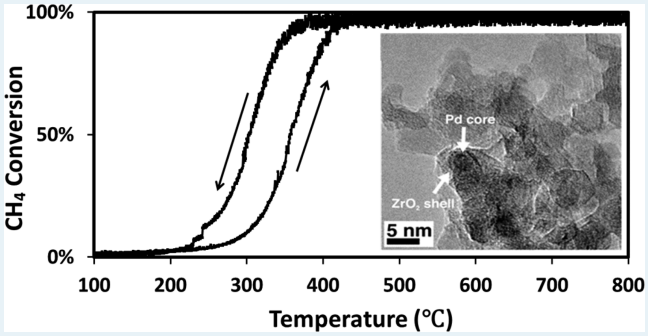

KEYWORDS: *methane oxidation, palladium, zirconia, core–shell catalysts, coulometric titration*

INTRODUCTION

The catalytic oxidation of methane has been extensively studied for applications ranging from removal of methane from engine exhausts to catalytic combustion for turbines, and supported PdO has been reported to be one of the best catalysts for this reaction.[1−7] However, major problems remain. First, the activity of conventional supported-Pd catalysts is insufficient at the lower temperatures, typically below 300 °C, required for applications with lean-burn engines,[1] especially in the presence of water vapor.[8,9] Second, metal sintering associated with high reaction temperatures leads to a loss of activity.

Our groups have recently demonstrated that a hierarchically structured catalyst, composed of $Pd@CeO_2$ nanoparticles supported on a functionalized Al_2O_3, shows great promise in solving some of these problems.[10] The catalysts were prepared using self-assembly methods, starting with 2 nm Pd particles dispersed in an organic solvent with thiol ligands, 11-mercaptoundecanoic acid (MUA). Dispersed $Pd@CeO_2$ particles were then prepared by reaction of cerium alkoxide with the acid functionality of the MUA ligand, followed by a controlled hydrolysis of the remaining alkoxide functionality in the presence of an organic acid. The core–shell particles were then adsorbed onto a functionalized Al_2O_3 support in monolayer form. After calcination to 850 °C to remove the ligands and activate the material, the catalyst showed very high activity for CH_4 oxidation at temperature below 400 °C and excellent thermal stability.

Unfortunately, the $Pd@CeO_2$ catalyst was also very sensitive to the presence of water in the reactant mixture. In addition to the inhibition observed for CH_4 oxidation in the presence of water vapor at lower temperatures, suggested as possibly being due to the reversible reaction of PdO to form $Pd(OH)_2$,[11,12] an additional deactivation of the $Pd@CeO_2$ catalyst was observed when CH_4 oxidation was carried out on the catalyst in the presence of water vapor at 600 °C.[13] Under these conditions, the CeO_2 shell was converted to a hydroxide that caused the rates to decrease dramatically by suppressing the transfer of oxygen from the support to the Pd. Catalyst activity could only be restored by heating the catalyst above 700 °C to decompose the hydroxide.

Received: June 26, 2014
Revised: September 23, 2014
Published: September 23, 2014

   dx.doi.org/10.1021/cs501146u | ACS Catal. 2014, 4, 3902−3909

Because water affects the performance of Pd@CeO_2/Si−Al_2O_3 catalyst by strong interaction with reduced ceria, it seemed possible that a core−shell catalyst with a different oxide shell could better resist water poisoning. An obvious choice for an alternative oxide shell is ZrO_2 because of its good hydrothermal stability.[9] Even though ZrO_2 is normally considered an irreducible oxide, and should therefore not promote reaction in the same way that CeO_2 does, there are some indications that interaction between Pd and ZrO_2 would affect the catalytic activity for CO hydrogenation,[14] methanol decomposition,[15] and methane steam reforming.[16] Furthermore, although the reaction order for CH_4 oxidation on Pd/ZrO_2 has been reported to be −1 in the H_2O partial pressure,[17] similar to what is observed on Pd/Al_2O_3,[9] another more recent study indicated that Pd/ZrO_2 showed superior performance for CH_4 oxidation in the presence of water vapor, even reporting "higher methane conversions in the presence of water vapor than in its absence".[18]

To determine the effect of the shell material on CH_4 oxidation, we set out to compare reaction rates on Pd@ZrO_2 and Pd@CeO_2. Interestingly, both catalysts exhibit nearly identical properties for CH_4 oxidation under dry conditions. Both Pd@ZrO_2 and Pd@CeO_2 catalysts exhibited higher rates after calcination to 800 °C compared to materials calcined to only 500 °C. Equilibrium redox measurements obtained from Coulometric titration indicated that the zirconia at the Pd interface could be reduced and helped stabilize the active PdO phase to lower P(O_2). Finally, the fact that Pd@ZrO_2 catalyst did not undergo deactivation during CH_4 oxidation in the presence of water vapor at 600 °C implies that this catalyst should be very interesting for this application.

EXPERIMENTAL METHODS

The synthesis of the Pd@ZrO_2/Si−Al_2O_3 catalyst is described in detail in previous publications.[10,19,20] Briefly, Pd@ZrO_2 core−shell nanoparticles were obtained by reaction of zirconium butoxide with 11-mercaptoundecanoic acid (MUA) protected Pd nanoparticles (Pd-MUA), followed by hydrolysis of zirconium butoxide to ZrO_2 in the presence of protective ligands. The Pd@ZrO_2 particles, dispersed in tetrahydrofuran, were then adsorbed from solution onto an Al_2O_3 support (hereafter referred to as Si−Al_2O_3) that had been modified by reaction with triethoxy octyl silane (TEOOS).[10] This modification of the support was required to make the Al_2O_3 hydrophobic so that Pd@ZrO_2 nanoparticles could adsorb onto the surface as isolated units. The Al_2O_3 itself was purchased from Alfa Aesar as γ-Al_2O_3 and then stabilized by calcining to 900 °C for 24 h, after which it had a surface area of 100 $m^2\ g^{-1}$ as determined by BET isotherms. Catalysts were prepared with ZrO_2:Pd weight ratios of either 6, 9, or 12; attempts to produce materials with higher ZrO_2/Pd ratios were not successful due to excess ZrO_2 that was not associated with Pd. The final catalysts were 1 wt % Pd. After removing the catalysts from solution by centrifugation and drying, the resulting Pd@ZrO_2/Si−Al_2O_3 powders were calcined to either 500 or 800 °C for 6 h with a heating ramp of 3 °C min^{-1}. Pd@CeO_2/Si−Al_2O_3 catalysts were produced in a similar way, with a CeO_2/Pd weight ratio of 9, and were also calcined to either 500 or 800 °C for 6 h using the same heating ramp.

Conventional Pd/ZrO_2 and Pd/Al_2O_3 catalysts were prepared by wet impregnation of $Pd(NH_4)_4(NO_3)_2$. The ZrO_2 support was obtained by thermal decomposition of $ZrO(NO_3)_2{\cdot}xH_2O$ at 750 °C. The Al_2O_3 support used here is the same material used for the supported core−shell catalysts except it was not modified by TEOOS. After impregnation, both catalysts were dried and calcined for 6 h to 500 °C. For comparison purposes, a 1 wt % Pd/Si−Al_2O_3 catalyst, prepared from the Pd-MUA particles without oxide shells and the TEOOS-functionalized Al_2O_3, was also synthesized. In this case, Si−Al_2O_3 powder was first dispersed in THF and then an appropriate amount of Pd-MUA nanoparticles was added to the mixture dropwise. After stirring overnight, the solid residue was recovered by centrifugation, dried and calcined to 800 °C for 6 h.

TEM characterization was performed on a Jeol JEM 2100 operating at 200 kV. Samples were prepared by dispersing the powders into isopropanol and by drop-casting of the dispersion onto holey carbon coated 300 mesh Cu grids. Powder X-ray diffraction (XRD) patterns were recorded on a Rigaku Smartlab diffractometer equipped with a Cu Kα source. The powders were finely dispersed in 2-propanol by sonication and then drop-cast onto glass slides before analysis.

The Pd dispersions were quantified by volumetric CO adsorption measurements at room temperature after the following pretreatments. The calcined samples were placed in the adsorption apparatus, heated in 200 Torr of O_2 at 400 °C, and then reduced at 150 °C in 200 Torr of H_2. Next, the samples were evacuated, cooled to room temperature, and then exposed to CO. O_2 titration measurements were performed in the same apparatus. In this case, the oxidized and reduced samples were heated in vacuum to 500 °C and then exposed to small pulses of O_2 until no additional O_2 was taken up by the sample.

Oxidation−reduction isotherms were measured using Coulometric titration, as described elsewhere.[21] The sample to be characterized was placed in an alumina crucible that was then inserted into a YSZ (yttria-stabilized zirconia) tube that had Ag electrodes painted on both inside and outside. The sample size was chosen so as to contain ∼100 μmoles of Pd. The entire apparatus was heated to 600 °C; and a mixture of 5% O_2, 11% H_2O, and 84% Ar was allowed to flow through the YSZ tube at this temperature for 1 h. After stopping the flow, the ends of the YSZ tube were sealed. To perform the actual measurements, oxygen was electrochemically pumped out of the YSZ tube by applying a potential across the electrodes with a Gamry instruments potentiostat. The amount of oxygen removed was determined by integrating the current as a function of time. After removing the desired amount of oxygen, the system was allowed to come to equilibrium with the electrodes at open circuit. The criterion that used for establishing equilibrium was that the open-circuit potential across the electrodes changed by less than 3 mV day^{-1}, which typically took between 4 and 10 days. Finally, the equilibrium P(O_2) was calculated from the Nernst equation and the open-circuit potential. As an additional check that equilibrium was achieved and that there were no system leaks, most isotherms were measured again starting with the reduced sample and pumping oxygen back into the electrochemical cell.

The pulse-reactor and light-off tests were performed in a tubular reactor that had an online quadrupole mass spectrometer to analyze the concentrations of the effluent gases.[22,23] Prior to loading the samples in the reactor, each was pressed into thin wafers that were then broken into smaller pieces. For pulse-reactor measurements, a 1 g sample was held in the quartz tubular reactor at atmospheric pressure. Computer-controlled solenoid valves allowed step changes in

dx.doi.org/10.1021/cs501146u | ACS Catal. 2014, 4, 3902−3909

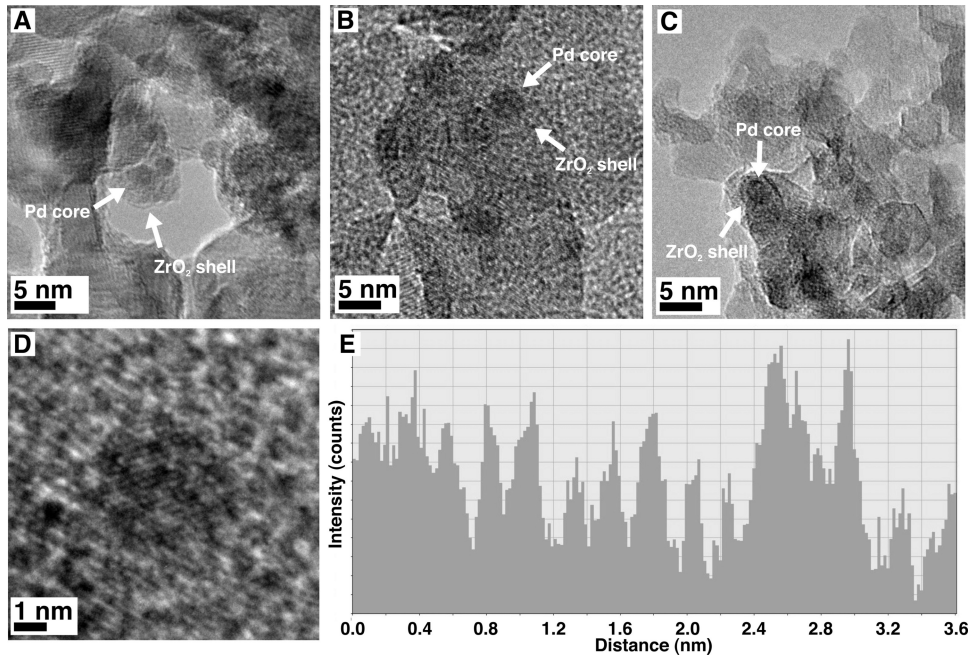

Figure 1. TEM images of Pd@ZrO_2/Si−Al_2O_3 catalysts. Panels A and B correspond to the 500 °C sample, whereas panel C pertains to the 800 °C calcined sample. In panels D and E, a lattice profile analysis of a single particle is presented.

the gas composition. In all cases, He was the majority component of the flow, and the concentration of the active component (CO or O_2) was maintained at 10%, with a total flow rate of 20 mL min^{-1}. Prior to the actual measurements, the samples were pretreated in O_2−He mixtures at 400 °C for 15 min, flushed with He for 10 min, and then reduced in CO-He for 15 min. The amount of CO_2 that formed during CO flow was quantified by integration of partial pressure of CO_2 as a function of time. This O_2−CO sequence was repeated three times to ensure the reproducibility of the redox properties of each sample.

The methane-oxidation, light-off tests used 400 mg of sample. The composition of the reactant mixture was chosen to be 1% CH_4 and 5% O_2 in He and the total flow rate was maintained at 120 mL min^{-1}. For those experiments in which H_2O was added, the reactant mixture was bubbled through a H_2O saturator, and the content of H_2O was controlled by the temperature of the saturator. Prior to performing a light-off measurement, each sample was exposed to a flowing mixture of 20% O_2 and 80% He for 30 min at 350 °C, then its temperature was ramped at 10 °C min^{-1} to 800 °C in 1% CH_4, 5% O_2, and 94% He, held at 800 °C for 1 h, and then cooled to room temperature at 10 °C min^{-1}. This last ramping of the sample temperature in the reactant mixture was followed because steady-state rate measurements showed that this procedure activated and stabilized the catalysts.

Steady-state rates for methane oxidation were measured using 100 mg of sample in a 1/4 in., quartz, flow reactor with an online gas chromatograph (SRI8610C) equipped with a Hayesep Q column and a TCD detector. For these measurements, the partial pressures of CH_4 and O_2 were fixed at 3.8 Torr (0.5%) and 38 Torr (5%), respectively, with a total flow rate of 120 mL min^{-1}, corresponding to Gas Hourly Space Velocity of 72 000 mL g^{-1} h^{-1}. CH_4 conversion was kept below 10% so that differential conditions could be assumed. The catalyst samples were again pressed into thin wafers, cleaned by oxidation at 350 °C in a flowing mixture of 20% O_2 and 80% He for 30 min, and activated by ramping the sample temperature in the reaction atmosphere to 800 °C.

RESULTS

TEM results for Pd@ZrO_2 catalysts prepared using the methods described here, with a 9:1 weight ratio of ZrO_2 to Pd, have been published previously.[20] Following calcination at 500 °C, uniform core−shell particles are formed, with Pd cores that are approximately 2 nm in diameter and ZrO_2 shells that are approximately 2 nm thick. Figures 1A,B show representative TEM images of the calcined, 1 wt % Pd, Pd@ZrO_2/Si−Al_2O_3 catalyst with this ZrO_2/Pd ratio after calcination at 500 °C. Because of the small Pd particle sizes and the low contrast between Pd and ZrO_2, these two components are not easily distinguishable in the TEM images. However, a few Pd particles were imaged and shown to be surrounded by a thin ZrO_2 layer (∼2 nm) in each case (Figure 1A,B). Even after calcination to 800 °C, a few small particles (2−3 nm), surrounded by a ZrO_2 layer, were found in the sample (Figure 1C). Due to the small particle size, it is hard to unequivocally attribute the lattice spacing to metallic or oxidized Pd phase. However, lattice profile analysis of individual particles in the samples calcined at 500 °C (Figure 1D,E) support a lattice spacing of ∼0.28 nm, in good agreement with the (101) lattice spacing in PdO (0.263 nm). It is likely that the low-temperature calcination treatment produces some form of PdO_x that reduces the contrast with the surrounding ZrO_2.

XRD patterns of Pd@ZrO_2/Si−Al_2O_3 catalysts with 1 wt % Pd and varying ZrO_2/Pd ratios, calcined to either 500 or 800 °C, are shown in Figure 2. The diffraction pattern of tetragonal zirconia phase is also provided for comparison. Not surprisingly, the patterns are dominated by features associated with Al_2O_3 and peaks associated with Pd are not visible in any of the patterns. More interesting is the fact that the only pattern exhibiting evidence for tetragonal ZrO_2, at 30.3 and 50.3 degrees 2θ, is the one with a ZrO_2/Pd ratio of 9, calcined at 800 °C, pattern 6. The ZrO_2 phase in all of the other samples is

dx.doi.org/10.1021/cs501146u | ACS Catal. 2014, 4, 3902−3909

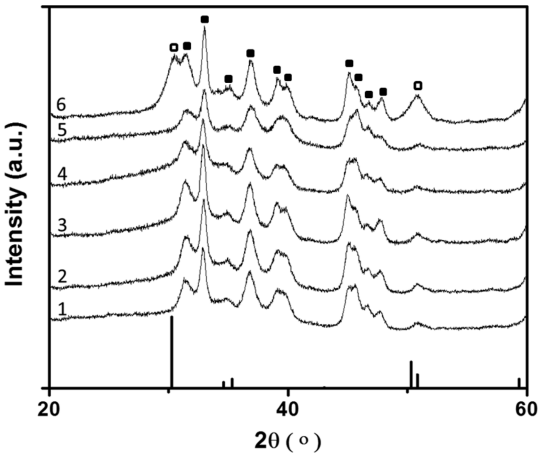

Figure 2. Powder XRD patterns of Pd/Si−Al_2O_3(1) and Pd@ZrO_2/Si−Al_2O_3 that calcined at different temperature and with different Pd/ZrO_2 ratio (2−6). 500 °C 1:6 (2), 500 °C 1:9 (3), 500 °C 1:12 (4), 800 °C 1:6 (5), 800 °C 1:9 (6). Reference powder diffraction pattern of tetragonal zirconia is shown at bottom. Al_2O_3 phase was marked by closed squares, ZrO_2 phase was marked with open squares.

either not crystalline or has crystallites too small to be observable by XRD. Even in pattern 6, the ZrO_2 crystallite sizes based on the peak width at half-maximum, calculated from the Scherrer equation, is only about 4 nm. Again, these results are consistent with formation of thin ZrO_2 shells in the Pd@ZrO_2 structures. At 800 °C and with 9 wt % ZrO_2, the shells are sufficiently thick to form crystallites large enough to be observable.

The metal dispersions, determined by CO chemisorption, are shown in Table 1 for the Pd@ZrO_2/Si−Al_2O_3 catalyst with 1 wt % Pd and 9 wt % ZrO_2, calcined at 500 and 800 °C. For the Pd catalyst prepared without a shell, the dispersion after heating to 500 °C in air was 30%. Because 2 nm Pd particles should have a dispersion of ∼50%, some sintering must have occurred during calcination. With the core−shell catalyst, the dispersion after heating to 500 °C in air is lower, ∼14%, due to the presence of the shell. The fact that adsorption is still observed implies that the shell must be porous. The CO chemisorption results were essentially unchanged after heating to 800 °C, suggesting that the core−shell helps stabilize the Pd particles, because heating to these high temperatures would normally be expected to cause Pd sintering.

Table 1. Pd Dispersions Based on CO Uptakes at Room Temperature

sample	dispersion (%)
1%Pd/Al_2O_3 500	30
1%Pd@ ZrO_2/Si−Al_2O_3 500	14
1%Pd@ ZrO_2/Si−Al_2O_3 800	13

Figure 3 shows steady-state rates for CH_4 oxidation on selected catalysts as a function of temperature, for 0.5% CH_4 and 5% O_2, under differential conditions. All of the samples contained 1 wt % Pd and exhibited similar activation energy, ∼90 kJ mol^{-1}. It is immediately apparent that the core−shell catalysts are significantly more active than the Pd/Al_2O_3 sample, despite having lower dispersions, implying that the ZrO_2 shell is not inert. Indeed, the methane-oxidation rates on the Pd@ZrO_2 samples were nearly identical to that observed previously with Pd@CeO_2/Si−Al_2O_3.[22] Also similar to what is observed on Pd@CeO_2/Si−Al_2O_3,[22] the rates improved when the samples were calcined to 800 °C, rather than 500 °C.

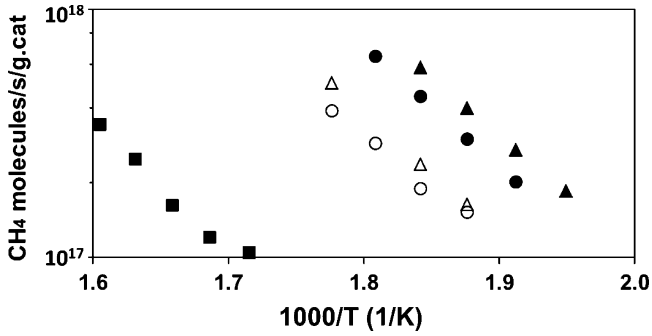

Figure 3. Rates for methane oxidation reaction over 1 wt %Pd/Al_2O_3 calcined at 500 °C (■), 1 wt %Pd@9 wt %CeO_2/Si−Al_2O_3 calcined at 500 °C (Δ), 1 wt %Pd@9 wt %ZrO_2/Si−Al_2O_3 calcined at 500 °C (○), 1 wt %Pd@9 wt %CeO_2/Si−Al_2O_3 calcined at 800 °C (▲), and 1 wt %Pd@9 wt %ZrO_2/Si−Al_2O_3 calcined at 800 °C (●). Data were taken with 0.5% CH_4 and 5% O_2.

A major issue observed with Pd@CeO_2/Si−Al_2O_3 catalyst is their strong sensitivity to the presence of water vapor in the feed.[13] Not only were the rates found to be much lower in the presence of water vapor, but carrying out CH_4 oxidation in the presence of water vapor at 600 °C resulted in a strong deactivation that could only be reversed by heating the sample above 700 °C. Results from previous work indicated that the CeO_2 shell formed a stable hydroxide that was unable to transfer oxygen to the Pd, causing the Pd to become reduced under reaction conditions. As shown in Figure 4, this deactivation process does not occur with the Pd@ZrO_2/Si−Al_2O_3 catalyst.

In Figure 4, the CH_4 conversion was measured as a function of temperature in 1% CH_4 and 5% O_2 as the temperature was ramped at 10 °C min^{-1} from 100 to 800 °C, then cooled at this same rate back to 100 °C. For the fresh samples calcined at 800 °C, results for Pd@ZrO_2/Si−Al_2O_3 and Pd@CeO_2/Si−Al_2O_3 are virtually identical. The conversion reached 100% by 400 °C

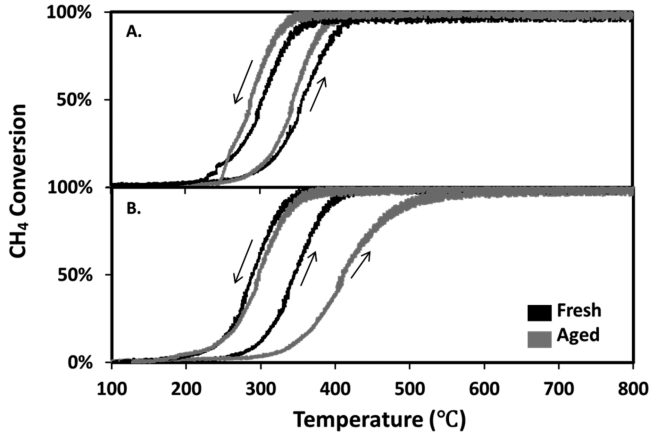

Figure 4. Effect of high temperature water poisoning over 1 wt %Pd@9 wt %ZrO_2/Si−Al_2O_3 (A) and 1 wt %Pd@9 wt %CeO_2/Si−Al_2O_3 (B). Both catalysts were calcined at 800 °C. The aged samples were kept under wet reaction conditions for 4 h at 600 °C, then cooled to room temperature under He, followed by light-off test. Data were taken with 1% CH_4 and 5% O_2. The heating and cooling rates are 10 °C min^{-1}.

dx.doi.org/10.1021/cs501146u | ACS Catal. 2014, 4, 3902−3909

on both catalysts on the upward ramp and showed a similar, ~50 °C shift to lower temperatures on the downward ramp. Under these conditions, there was also no evidence for a decrease in conversion at higher temperature due to a PdO-Pd transformation, typically observed near 600 °C. However, when the catalysts were aged for 4 h at 600 °C in 1% CH_4, 5% O_2, and 10% H_2O, the results for Pd@ZrO_2/Si−Al_2O_3 and Pd@CeO_2/Si−Al_2O_3 were very different. After this pretreatment, the light-off curve for Pd@CeO_2/Si−Al_2O_3 in a dry reactant stream was shifted by more than 50 °C to higher temperatures on the upward ramp. After heating to 800 °C, the conversions on the downward ramp were the same as with the freshly calcined sample due to decomposition of the hydroxides. With Pd@ZrO_2/Si−Al_2O_3, aging under wet conditions had no effect.

Rates on the Pd@ZrO_2/Si−Al_2O_3 catalyst also seem to be less affected in the presence of water. Figure 5 compares light-off curves on the same two catalysts but now with 10% H_2O in the reactant mixture. For both catalysts, there is a shift to higher temperatures when H_2O is present. However, the shift is less with Pd@ZrO_2/Si−Al_2O_3. On the upward ramp, the CH_4 conversion reaches 100% at 500 °C on Pd@ZrO_2/Si−Al_2O_3, but this conversion was reached with Pd@CeO_2/Si−Al_2O_3 only after heating to 600 °C.

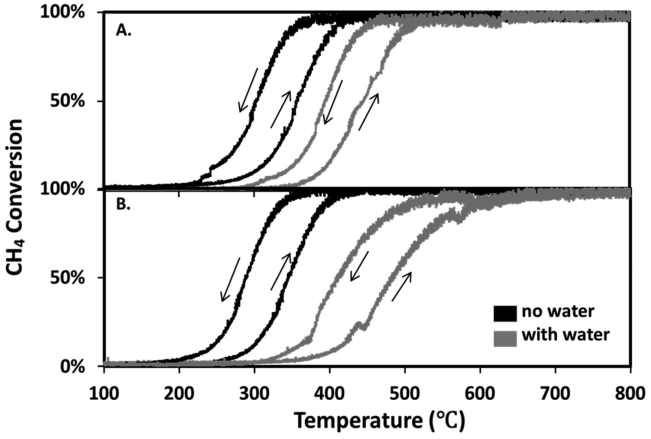

Figure 5. Effect of water on methane light-off curves over 1 wt %Pd@9 wt %ZrO_2/Si−Al_2O_3 (A) and 1 wt %Pd@9 wt %CeO_2/Si−Al_2O_3 (B). Both catalysts were calcined at 800 °C. Data were taken with 1% CH_4, 5% O_2, and 10% H_2O (if present). The heating and cooling rates are 10 °C min^{-1}.

Although there are differences between the catalysts made with CeO_2 and ZrO_2 shells, the similarities are perhaps more surprising. CeO_2 is well-known to promote a wide range of reactions due to its reducibility,[24] but ZrO_2 is normally considered an irreducible oxide. Because some reports have suggested ZrO_2 in contact with metals can be reduced,[23,25−27] we examined the redox properties of our catalysts.

Results from pulse-reactor and oxygen-titration studies are shown in Table 2 for a series of catalysts with 1 wt % Pd. In the pulse measurements, the samples were exposed to a series of CO and O_2 pulses at 400 °C, and the amount of CO_2 formed during the CO pulse was then quantified. If any of the CO_2 that is formed is due to the Bouduard reaction, CO_2 would be formed during the O_2 pulse, which was not observed. For a 1 wt % Pd catalyst, 94 μmol of CO_2/g of catalyst can be formed by reduction of PdO to Pd. For the conventional Pd/ZrO_2 catalyst and for the Pd nanoparticles on the functionalized Si−Al_2O_3, the amount of oxygen that could be removed was within

Table 2. Results of O_2 Titration and Pulse Study on Different Pd-Based Samples Used in This Study

	sample	reducibility (μmol O/g_{sample})
CO-O_2-CO pulse study	Pd/Si−Al_2O_3	107
	Pd/ZrO_2	95
	Pd@ ZrO_2/Si−Al_2O_3 1:6 500	160
	Pd@ ZrO_2/Si−Al_2O_3 1:9 500	154
	Pd@ ZrO_2/Si−Al_2O_3 1:12 500	145
	Pd@ ZrO_2/Si−Al_2O_3 1:9 800	145
O_2 titration	Pd/Si−Al_2O_3	87
	Pd@ZrO_2/Si−Al_2O_3 1:6 500	148

experimental uncertainty of this value. However, for the core−shell catalyst, significantly more oxygen, between 145 and 160 μmol/g, was removed from the samples than could be explained by reduction of PdO. This was true for samples calcined at both 500 and 800 °C. The added amount of oxygen was not dependent on the amount of ZrO_2 in the sample, suggesting that only ZrO_2 that was in contact with the Pd was affected. To confirm these results, O_2 titration measurements were performed in the volumetric apparatus on the Pd/Si−Al_2O_3 and Pd@ZrO_2/Si−Al_2O_3 (calcined at 500 °C, with a ZrO_2:Pd ratio of 6) samples. In addition to using a different apparatus, the O_2 titration measurements used H_2 at 500 °C to reduce the catalysts and measured the amount of O_2 that could be taken up by the reduced samples. The results were in reasonable agreement with the pulse data.

To gain additional insight into the redox properties of the core−shell catalysts, Coulometric titration experiments were performed. In Coulometric titration, a known amount of oxygen is first electrochemically pumped in or out of a sealed vessel containing the sample. After allowing the sample to reach equilibrium, the $P(O_2)$ is retrieved by measuring the voltage across a YSZ electrolyte.[28,29] Figure 6A shows results at 600 °C for Pd/Al_2O_3 catalysts with 1% and 5% Pd loading. The amount of oxygen removed from the samples, relative to the Pd content, is plotted against the equilibrium $P(O_2)$. Starting from the oxidized catalyst, the $P(O_2)$ at which PdO is completely reduced to Pd was found to be ~3.5×10^{-3} atm, in reasonable agreement with standard thermochemical data, which indicates the equilibrium $P(O_2)$ for the PdO-Pd transformation being 2.0×10^{-3} atm.[30] Because no other compounds can influence the $P(O_2)$ at this point, removal of even small amounts of oxygen causes the $P(O_2)$ to decrease to very low levels. It is worth noting that results for 1 wt % and 5 wt % Pd were identical, demonstrating that the Pd loading does not influence the thermodynamics of the PdO-Pd reduction.

The analogous data for a conventional 1 wt % Pd/ZrO_2 catalyst, given in Figure 6B, indicate that much more oxygen can be removed from this sample than from the 1 wt % Pd/Al_2O_3 catalyst and that reduction occurs in two stages. A reduction step with an O/Pd stoichiometry of 1 occurs between 10^{-3} and 10^{-4} atm as observed in the case of the Pd/Al_2O_3 sample, indicating that the support does not influence the thermodynamics of the PdO-Pd reduction. In addition to this first reduction, there is a second process observed at a $P(O_2)$ of about 10^{-20} atm. This second step must be associated with

dx.doi.org/10.1021/cs501146u | ACS Catal. 2014, 4, 3902−3909

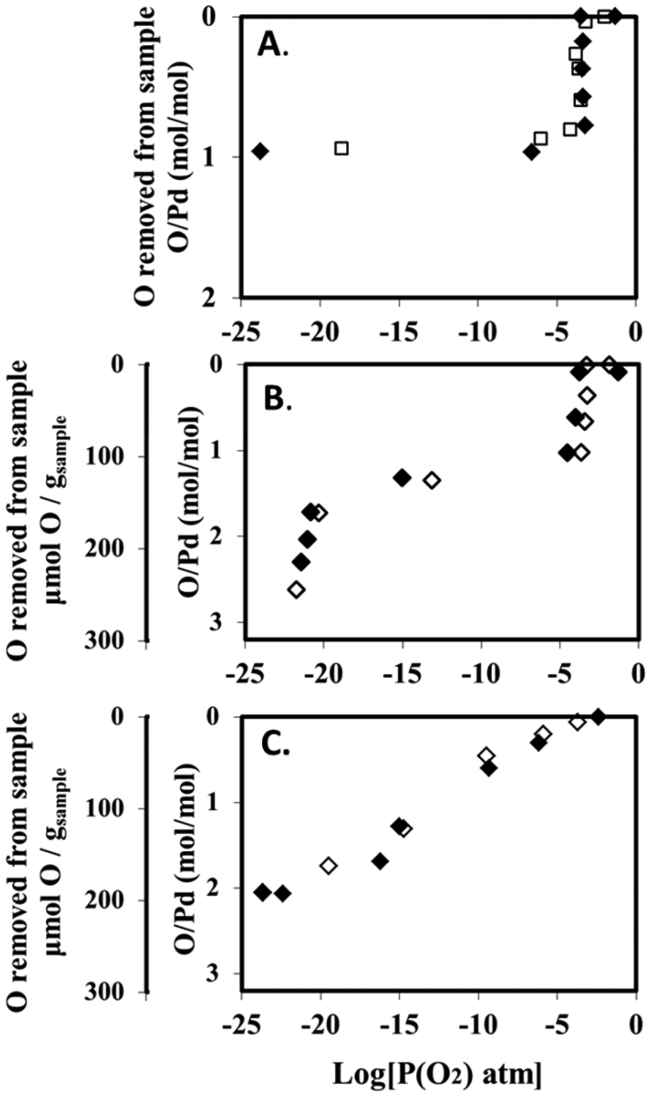

Figure 6. Redox isotherms for Pd/Al_2O_3 (A) with 1 wt % Pd (□) and 5 wt % Pd (◆), 1 wt % Pd/ZrO_2 (B), and 1 wt % Pd@9 wt %ZrO_2/$Si-Al_2O_3$ (C). ◆ symbols were obtained starting from the oxidized state. ◊ symbols were measured while reoxidizing the sample. All measurements were conducted at 600 °C.

reduction of the support. The isotherms measured in both directions (e.g., starting from an oxidized or a reduced sample) demonstrated good reproducibility. In contrast to pulse studies (see above), reduction can be observed in the Coulometric titration experiment because of the very reducing conditions that can be achieved with this technique at higher temperature (600 °C compared to 400 °C in the pulse study). It should be noted that, even with these more severe conditions, only a small fraction of the ZrO_2 phase is reduced. Indeed, the extent of reduction is consistent with only the oxide at the Pd-ZrO_2 interface being reduced.

The results for the 1 wt % Pd@ZrO_2/$Si-Al_2O_3$ catalyst, with a ZrO_2/Pd ratio of 9, after calcination to 800 °C, were very different from those of the previous two samples (Figure 6C). First, the amount of oxygen that could be removed from the sample was greater than that observed in the pulse experiments because of the higher temperatures used in the Coulometric titration experiments. The total amount of oxygen removed from this sample in Coulometric titration was approximately 2 mol per mole of Pd. (Even so, the average oxygen stoichiometry of the zirconia phase never had a calculated O/Zr ratio less than 1.89.) Also, unlike the isotherms on the conventional catalysts, there is no well-defined step at $\sim 10^{-3}$ atm corresponding to equilibrium between Pd and PdO. Reduction occurs over a wide range of $P(O_2)$ and reduction of both the PdO and the ZrO_2 shell appears to occur in single, gradual process. The reversibility of the isotherms demonstrates that these results are not simply due to kinetic effects but to thermodynamic properties of the sample.

An important consideration for interpreting the results from Coulometric titration is that the samples are exposed to reducing conditions at 600 °C for long periods of time. Measurement of complete isotherms like those in Figure 6A–C typically takes 60 days. For the conventional supported-Pd catalysts, significant sintering of the metal phase occurred during this time. At the end of the experiments, the Pd dispersions for the Pd/Al_2O_3 and Pd/ZrO_2 catalysts were both determined to be below 3%. By comparison, the Pd@ZrO_2/$Si-Al_2O_3$ was affected to a much lesser extent. Even after this treatment, the dispersion was determined to be ~8% by CO chemisorption, suggesting that the Pd had not grown larger than the original 2 nm.

DISCUSSION

A number of potentially important observations can be drawn from the results of this study. First, Pd@ZrO_2, core–shell catalysts are promising materials for CH_4 oxidation catalysis. The activity of these materials is comparable to the Pd@CeO_2 catalysts, without exhibiting the same deactivation in water vapor that was observed with the CeO_2-based catalyst. Second, ZrO_2 appears to be reducible, at least when it is in contact with Pd. The extent of ZrO_2 reduction is less than that observed with CeO_2 and it may be that only the ZrO_2 in direct contact with Pd is reduced; however, the fact that ZrO_2 may be able to donate oxygen to the metal under reaction conditions may explain why ZrO_2 catalyst can be catalytically active. Third, stabilization of PdO phase in the core–shell structure is demonstrated by showing that the equilibrium $P(O_2)$ for the Pd-PdO transition is shifted to much lower values compared to those measured on convertional Pd/ZrO_2. Fourth, the equilibrium oxidation–reduction properties of the Pd@ZrO_2 core–shell catalysts are not a simple sum of those expected for the individual PdO-Pd and ZrO_2 phases. These four observations may indeed be related.

It has long been proposed that CeO_2-supported catalysts derive some of their attractive properties because of the reducibility of CeO_2, with oxygen transfer from CeO_2 to the metal playing an important part.[31,32] Indeed, a very recent study of CO oxidation on CeO_2-supported Pt, Pd, and Ni catalysts showed a strong correlation between rates and the interfacial contact area between the metal and CeO_2.[33] Maximizing the contact area between the transition metal and CeO_2 was a fundamental goal behind preparing Pd@CeO_2 core–shell catalysts.[10] Based on the present results with Pd@ZrO_2, it appears that a similar process may be applicable with the ZrO_2 analog as well. Transfer of oxygen from ZrO_2 to the Pd may occur under reaction conditions.

Contact between the transition metal and ZrO_2 in these core–shell materials may also provide opportunities that are not available with CeO_2. The Ce(III)–Ce(IV) redox couple is strongly dependent on the local structure and Ce cations can get locked into one oxidation state or the other depending on

dx.doi.org/10.1021/cs501146u | ACS Catal. 2014, 4, 3902–3909

the local composition and structure. For example, in $CeVO_3$, Ce is locked in the +3 oxidation state; it has been reported that even exposure to oxygen plasmas is not able to oxidize the Ce cations.[34] By contrast, well-crystallized CeO_2 is difficult to reduce.[35] The primary reason that ceria−zirconia mixed oxides must be used for oxygen storage in three-way, automotive catalysts is that pure ceria loses its redox properties over time.[24] In the case of Pd@CeO_2 catalysts aged in water vapor, it appears that the CeO_2 shell converts to the hydroxide, which likely has Ce in its +3 state. The fact that ZrO_2 does not form the stable reduced phases under normal conditions may provide an opportunity in that it is unlikely that ZrO_2 would be similarly locked in a reduced state.

It is generally accepted that PdO is the active phase for methane oxidation over Pd-based catalysts. Thermal decomposition of PdO to less active Pd at high temperatures plays an important role in affecting its reactivity. The results of coulometric titration show a significant shift to lower $P(O_2)$ for the equilibrium state associated with PdO−Pd transformation, suggesting the metal−oxide interaction between Pd and ZrO_2 strongly enhanced PdO stability which in turn improved the catalytic activity.

It is intriguing that the coulometric titration data for the Pd@ZrO_2 catalyst did not exhibit a step at the expected $P(O_2)$ where PdO and Pd should be in equilibrium and that there was no distinct ranges that could be identified as reduction of Pd or reduction of ZrO_2. In regards to reduction of PdO, it is possible that surface energies could influence the thermodynamics of the nanoparticles. For example, it has been reported that small supported Co particles can become oxidized under conditions used for the Fischer−Tropsch reaction, even though bulk thermodynamics suggest that metallic Co should be the stable phase.[36] Theoretical considerations have shown that the surface energies of nanoparticle Co are large enough to explain this effect.[37] Although an experimental attempt to verify this effect did not observe changes in the equilibrium $P(O_2)$ as a function of particle size, shifts to lower values were observed for the equilibrium $P(O_2)$ for small particles interacting with ZrO_2.[38] That study suggested that Co-ZrO_2 interactions could be modifying the equilibrium properties. In principle, Pd-ZrO_2 interactions could be causing similar effects. Finally, it is noteworthy that metallic Zr can form very stable alloys with precious metals, referred to as Engel−Brewer intermetallic,[39,40] and this could provide a driving force for reduction of ZrO_2. Again, some evidence for this has been presented in the literature for Pt.[28,41]

Finally, the fact that the Pd@ZrO_2 catalyst maintained its Pd dispersion to a much greater level after being exposed to reducing conditions at 600 °C for 60 days is a potentially important observation. As reported previously for Pd@CeO_2, these core−shell catalysts appear to exhibit special stability based on their hierarchical structure. This property is obviously very important for high-temperature applications, such as methane oxidation.

There are still many unresolved question about the unique properties of Pd@ZrO_2/Si−Al_2O_3 catalysts that need to be further investigated. However, their high activity for methane oxidation, good thermal stability, and high resistance toward water poisoning demonstrate the great potential for real catalytic application.

CONCLUSION

In the Pd@ZrO_2 core−shell catalyst, PdO phase was stabilized through strong interaction between Pd core and ZrO_2 shell. The ZrO_2 in contact with Pd is reducible and appears to enhance the oxidation activity of the Pd in a manner similar to what is observed with CeO_2. However, the ZrO_2 shell is distinct from CeO_2 in not undergoing deactivation in the presence of steam at high temperatures. Similar to earlier observations with Pd@CeO_2, the Pd@ZrO_2 catalysts also exhibit good thermal stability against sintering.

AUTHOR INFORMATION

Corresponding Author

*E-mail: chenc5@seas.upenn.edu.

Notes

The authors declare no competing financial interest.

ACKNOWLEDGMENTS

C.C. and R.J.G. were supported by the Department of Energy, Office of Basic Energy Sciences, Chemical Sciences, Geosciences and Biosciences Division, Grant No. DE-FG02-13ER16380. M.C. acknowledges support from the National Science Foundation through the Nano/Bio Interface Center at the University of Pennsylvania, Grant DMR08-32802. C.B.M. is grateful for the support of the Richard Perry University Professorship. P.F. acknowledges COST Action CM1104 “Reducible oxide chemistry, structure, and functions” and University of Trieste through FRA 2013 project.

REFERENCES

(1) Farrauto, R. J. *Science* **2012**, *337*, 659−660.
(2) Forzatti, P.; Groppi, G. *Catal. Today* **1999**, *54*, 165−180.
(3) Forzatti, P. *Catal. Today* **2003**, *83*, 3−18.
(4) Ciuparu, D.; Lyubovsky, M. R.; Altman, E.; Pfefferle, L. D.; Datye, A. *Catal. Rev.* **2002**, *44*, 593−649.
(5) Kucharczyk, B.; Tylus, W.; Kepinski, L. *Appl. Catal., B* **2004**, *49*, 27−37.
(6) Gelin, P.; Primet, M. *Appl. Catal., B* **2002**, *39*, 1−37.
(7) Farrauto, R. J.; Hobson, M. C.; Kennelly, T.; Waterman, E. M. *Appl. Catal., A* **1992**, *81*, 227−237.
(8) Schwartz, W. R.; Ciuparu, D.; Pfefferle, L. D. *J. Phys. Chem. C* **2012**, *116*, 8587−8593.
(9) Gholami, R.; Alyani, M.; Smith, K. J. *Catalysts* **2014**, *4*, 1 DOI: 10.3390/catal40x000x.
(10) Cargnello, M.; Jaen, J. J. D.; Garrido, J. C. H.; Bakhmutsky, K.; Montini, T.; Gamez, J. J. C.; Gorte, R. J.; Fornasiero, P. *Science* **2012**, *337*, 713−717.
(11) Ribeiro, F. H.; Chow, M.; Dallabetta, R. A. *J. Catal.* **1994**, *146*, 537−544.
(12) Fujimoto, K.; Ribeiro, F. H.; Avalos-Borja, M.; Iglesia, E. *J. Catal.* **1998**, *179*, 431−442.
(13) Monai, M.; Montini, T.; Chen, C.; Fonda, E.; Gorte, R. J.; Fornasiero, P. *ChemCatChem* **2014**, DOI: 10.1002/cctc.201402717, submitted for publication.
(14) Shen, W. J.; Okumura, M.; Matsumura, Y.; Haruta, M. *Appl. Catal., A* **2001**, *213*, 225−232.
(15) Usami, Y.; Kagawa, K.; Kawazoe, M.; Matsumura, Y.; Sakurai, H.; Haruta, M. *Appl. Catal., A* **1998**, *171*, 123−130.
(16) Hegarty, M. E. S.; O'Connor, A. M.; Ross, J. R. H. *Catal. Today* **1998**, *42*, 225−232.
(17) Araya, P.; Guerrero, S.; Robertson, J.; Gracia, F. J. *Appl. Catal., A* **2005**, *283*, 225−233.
(18) Park, J.-H.; Cho, J. H.; Kim, Y. J.; Kim, E. S.; Han, H. S.; Shin, C.-H. *Appl. Catal., B* **2014**, *160−161*, 135−143.

(19) Cargnello, M.; Wieder, N. L.; Montini, T.; Gorte, R. J.; Fornasiero, P. *J. Am. Chem. Soc.* **2010**, *132*, 1402−1409.
(20) Bakhmutsky, K.; Wieder, N. L.; Cargnello, M.; Galloway, B.; Fornasiero, P.; Gorte, R. J. *ChemSusChem* **2012**, *5*, 140−148.
(21) Baldychev, I.; Gorte, R. J.; Vohs, J. M. *J. Catal.* **2010**, *269*, 397−403.
(22) Chen, C.; Cao, J. J.; Cargnello, M.; Fornasiero, P.; Gorte, R. J. *J. Catal.* **2013**, *306*, 109−115.
(23) Sharma, S.; Hilaire, S.; Vohs, J. M.; Gorte, R. J.; Jen, H. W. *J. Catal.* **2000**, *190*, 199−204.
(24) Gorte, R. J. *AIChE J.* **2010**, *56*, 1126−1135.
(25) Stagg, S. M.; Romeo, E.; Padro, C.; Resasco, D. E. *J. Catal.* **1998**, *178*, 137−145.
(26) Zhang, X.; Shi, H.; Xu, B. Q. *Angew. Chem., Int. Ed.* **2005**, *44*, 7132−7135.
(27) Claus, P.; Bruckner, A.; Mohr, C.; Hofmeister, H. *J. Am. Chem. Soc.* **2000**, *122*, 11430−11439.
(28) Shah, P. R.; Kim, T.; Zhou, G.; Fornasiero, P.; Gorte, R. J. *Chem. Mater.* **2006**, *18*, 5363−5369.
(29) Shah, P. R.; Khader, M. M.; Vohs, J. M.; Gorte, R. J. *J. Phys. Chem. C* **2008**, *112*, 2613−2617.
(30) Barin, I. *Thermochemical Data of Pure Substances, Part I and II*; Wiley VCH: Weinheim, Germany, 1989; pp 1093−1168.
(31) Cordatos, H.; Bunluesin, T.; Stubenrauch, J.; Vohs, J. M.; Gorte, R. J. *J. Phys. Chem.* **1996**, *100*, 785−789.
(32) Bunluesin, T.; Gorte, R. J.; Graham, G. W. *Appl. Catal., B* **1997**, *14*, 105−115.
(33) Cargnello, M.; Doan-Nguyen, V. V. T.; Gordon, T. R.; Diaz, R. E.; Stach, E. A.; Gorte, R. J.; Fornasiero, P.; Murray, C. B. *Science* **2013**, *341*, 771−773.
(34) Reidy, R. F.; Swider, K. E. *J. Am. Ceram. Soc.* **1995**, *78*, 1121−1122.
(35) Zhou, G.; Shah, P. R.; Montini, T.; Fornasiero, P.; Gorte, R. J. *Surf. Sci.* **2007**, *601*, 2512−2519.
(36) Bezemer, G. L.; Bitter, J. H.; Kuipers, H. P. C. E.; Oosterbeek, H.; Holewijn, J. E.; Xu, X. D.; Kapteijn, F.; van Dillen, A. J.; de Jong, K. P. *J. Am. Chem. Soc.* **2006**, *128*, 3956−3964.
(37) van Steen, E.; Claeys, M.; Dry, M. E.; van de Loosdrecht, J.; Viljoen, E. L.; Visagie, J. L. *J. Phys. Chem. B* **2005**, *109*, 3575−3577.
(38) Bakhmutsky, K.; Wieder, N. L.; Baldassare, T.; Smith, M. A.; Gorte, R. J. *Appl. Catal., A* **2011**, *397*, 266−271.
(39) Saida, J.; Matsushita, M.; Inoue, A. *J. Appl. Phys.* **2001**, *90*, 4717−4724.
(40) Wang, H.; Carter, E. A. *J. Am. Chem. Soc.* **1993**, *115*, 2357−2362.
(41) Werner, J.; Schmidfetzer, R. *Thermochim. Acta* **1988**, *129*, 127−141.